Proton Acceleration from High-Intensity Laser Interactions with Thin Foil Targets

M. Zepf,[1,*] E. L. Clark,[2,3] F. N. Beg,[2] R. J. Clarke,[4] A. E. Dangor,[2] A. Gopal,[2] K. Krushelnick,[2] P. A. Norreys,[4] M. Tatarakis,[2] U. Wagner,[4] and M. S. Wei[2]

[1]*Department of Physics, The Queen's University, University Road, Belfast, BT7 1NN, United Kingdom*
[2]*Blackett Laboratory, Imperial College of Science, Technology, and Medicine, London SW7 2BZ, United Kingdom*
[3]*Plasma Physics Department, AWE plc, Aldermaston, Reading RG7 4PR, United Kingdom*
[4]*Rutherford Appleton Laboratory, Chilton, Didcot, Oxon OX11 OQX, United Kingdom*

(Received 7 February 2002; published 13 February 2003)

Measurements of energetic proton production resulting from the interaction of high-intensity laser pulses with foil targets are described. Through the use of layered foil targets and heating of the target material we are able to distinguish three distinct populations of protons. One high energy population is associated with a proton source near the front surface of the target and is observed to be emitted with a characteristic ring structure. A source of typically lower energy, lower divergence protons originates from the rear surface of the target. Finally, a qualitatively separate source of even lower energy protons and ions is observed with a large divergence. Acceleration mechanisms for these separate sources are discussed.

DOI: 10.1103/PhysRevLett.90.064801 PACS numbers: 41.75.Jv, 29.30.Ep, 52.70.Nc

Particle acceleration using high-intensity laser-produced plasmas has been the subject of a significant amount of recent research [1]. This is primarily due to the large electric fields which can be supported in a plasma which may enable a reduction in the size and cost of future particle accelerators. One particular observation [2]—that of an intense beam of energetic protons (tens of MeV) emerging from the rear of thin foil targets during interactions with high-intensity laser pulses—has sparked a significant amount of work by various groups [3–5].

Experimental measurements of angular distribution and energy of these protons have been generally consistent, however there is still debate with regard to the origin of the protons and the precise acceleration mechanism. In this paper we will briefly explain the physical processes that give rise to the accelerating field and then discuss the experimental observations that have led one mechanism to be preferred over another in the interpretation of past experiments. We then present the first measurements that allow the contributions from the various acceleration mechanisms to be distinguished and classify them according to their angular emission profiles.

Acceleration mechanisms which have been suggested include sheath acceleration which generates large electric fields at the rear of the target [3] and fields set up at the front or inside the target [2,4]. The origin of the accelerating field at the rear of the target is readily understood. During the interaction the high-intensity laser light couples its energy efficiently into a beam of fast electrons. These fast electrons then propagate to the rear of the target and set up a strong electrostatic field upon exiting which forces the electrons back into the target and drags protons and ions out of the target.

Charge separation also occurs at the critical surface over short distances at the front of the target, due to the ponderomotive force of the laser pulse. This accelerates protons to approximately the ponderomotive energy of the laser (≈ 4 MeV for 10^{20} W cm^{-2}) as a result of hole boring and/or the propagation of an electrostatic shock [6]. Toupin *et al.*, for example, predict a collimated, multi-MeV ion beam that is directed into the target for small density scale lengths [7]—predictions that are supported by some experimental evidence [8]. The predicted ion energies are low compared to those that have been observed to emerge from the rear of the target, but these acceleration processes may be the origin of some of the fastest protons that receive an initial kick and that are accelerated more efficiently in subsequent fields [9].

As the electron beam propagates into the target, the current must be compensated by a suitable return current. An electric field is required to drive this return current. Since the electron beam is generated at the critical surface and its density is therefore much lower than that of the solid, the return current will be provided by a slow drift of the background electrons. These will be strongly affected by collisions and the resulting electric field can be estimated from the target resistivity [9–11]. Even in good conductors the current density generated by high-intensity lasers leads to a significant electric field. Such fields can extend over relatively large distances (the penetration depth of the hot electron beam) and their magnitude depends strongly on the resistivity experienced by the return current.

Present computational modeling of these plasmas is only of limited use in elucidating the question of the relative strength of the accelerating electric fields. Particle-in-cell codes (PIC) frequently do not include collisions, assume that the plasma is already hot (electron temperature ~ 1 keV) for numerical reasons and at $\sim 1/10$ of solid density to reduce computation time.

By contrast the target is initially a cold solid in the experiments. Consequently there is some doubt as to the validity of PIC simulations for predicting material conditions and electron transport inside a target which is rapidly evolving from a cold solid to hot dense plasma. However, PIC codes typically provide accurate predictions for high-intensity short pulse laser experiments in low density plasmas or at surfaces of solid targets [12,13]. Results from three dimensional simulations [13] show protons accelerated up to 6 MeV for $I\lambda^2 = 10^{19}\ \mathrm{W\,cm^{-2}}\,\mu\mathrm{m}^2$, by fields at the rear of the target, where the PIC code should be reasonably accurate. This is lower than the experimental observation of 10 MeV at $6 \times 10^{18}\ \mathrm{W\,cm^{-2}}\,\mu\mathrm{m}^2$ and 20 MeV at $10^{19}\ \mathrm{W\,cm^{-2}}\,\mu\mathrm{m}^2$. They also predict a divergence of around 10° full width angle for the lower energy protons rather than the 40°–60° observed experimentally.

Alternative modeling techniques such as hybrid PIC/fluid codes [11] are capable of capturing the transition from cold solid to plasma and do predict large accelerating electric fields in the target. The observation of collimated electron transport both experimentally [14] and in the hybrid codes [11] suggests that this approach may qualitatively capture the physical processes inside the target. The fields predicted to exist inside the target are, however, not large enough to explain the large proton energies observed experimentally. Since the resistivity is not calculated self-consistently (typically approximated by the Spitzer expression), the code may well underestimate the magnitude of the fields. Effects such as the lower hybrid instability [15] are expected to result in enhanced resistivity and thus higher field strengths.

The most direct evidence for the origin of the protons and the acceleration mechanism involved comes from experiments by Maksimchuk *et al.* [4]. The deuterium induced activation of a boron sample positioned at the rear of a thin foil target was measured. During laser interactions in the intensity range of $I\lambda^2 = 5 \times 10^{17}$–$6 \times 10^{18}\ \mathrm{W\,cm^{-2}}\,\mu\mathrm{m}^2$ such activation was observed only when the front surface was coated with deuterium. Furthermore, the energy of protons was found to increase with increasing target thickness in the range of 0.1–10 μm, which is consistent with an acceleration mechanism near the front of the target. The internal field gradient inferred from these measurements is $\sim 10^{11}\ \mathrm{V\,m^{-1}}$ for $I\lambda^2 = 5 \times 10^{17}\ \mathrm{W\,cm^{-2}}\,\mu\mathrm{m}^2$, and is substantially higher than hybrid codes predict.

On the other hand, the proton beam tends to be aligned to the rear target surface normal in most experiments and experiments using wedge shaped targets have observed a proton beam from both rear surfaces [3]. This suggests that the rear surface strongly influences the proton acceleration and that acceleration directly from the rear surface may dominate. Further support for this hypothesis has come from recent experiments which show that the proton beam can be suppressed by forming a plasma on the rear surface [16].

Clearly, it is possible that several acceleration mechanisms are operating simultaneously. A fundamental difficulty is to measure the various acceleration mechanisms independently. In a typical experiment, hydrogen is present on all target materials in the form of surface contaminants (and possibly trapped within the lattice structure of the target), which makes it difficult to determine the various contributions.

The results presented here were obtained using the Vulcan laser at the Rutherford Appleton Laboratory. This laser delivers 80 J pulses in 0.8–1.2 ps at a wavelength of 1.054 μm. The beam was p polarized and was focused to a maximum intensity of about $8 \times 10^{19}\ \mathrm{W\,cm^{-2}}$. The protons were detected using stacks of CR39 nuclear track detectors, radio-chromic film (RCF), and materials for nuclear activation. Since the protons are decelerated as they pass through subsequent layers of the detector stack, one can obtain images of the proton angular distributions at different energies on a single shot [2].

The approach taken in the experiment described here is to selectively contaminate one side of the target with hydrogen by coating it with a suitable compound while minimizing the general hydrocarbon surface contamination by heating the target. The temperature at which all surface contamination boils off reliably is in excess of 1000 °C [17]. Unfortunately, such temperatures are above the typical boiling point of most hydrocarbon compounds, which could be used to coat the target. Consequently, the temperature was chosen as a compromise between boiling off the contaminants while retaining the coating. Therefore, some contamination is still present on all surfaces during the experiment. The target temperature was typically 300–400 °C. At this temperature we observed that the hydrocarbon contamination was significantly reduced and the integrity of the coating was maintained. The coating consisted of PEEK (Polyetheretherketone), which has a melting point of 350 °C but retains a high viscosity far beyond the melting point. Figure 1 shows a comparison of the ion spectra taken from a heated and an unheated pure aluminum target showing a significant reduction in the overall proton signal.

Our measurements indicate that this reduction of the contamination is sufficient to distinguish between the signal from the front and the back. Figures 2(a)–2(c) show typical proton data recorded with RCF and CR39 detector stacks from an interaction with a square, unheated Al target of 100 μm thickness. The features can be categorized into three qualitatively distinct regions. First, there is a crosslike pattern that extends to very large angles from the center of symmetry. Second, there is a ring of enhanced signal which is clearly visible on the CR39 track detector data, and third, there is a feature at the center of the ring that corresponds to the area of highest exposure on the RCF. The ring structure contracts with increasing proton energy, while the feature at the

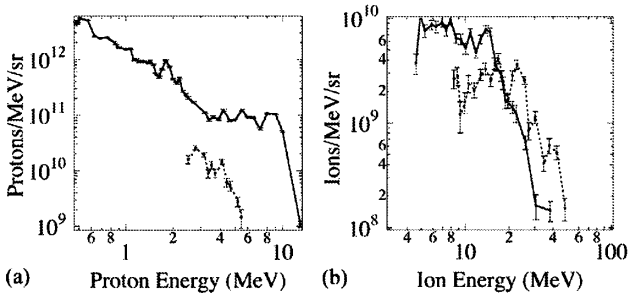

FIG. 1. (a) Comparison of proton spectra from the heated (dotted line) and unheated Al targets (solid line). (b) Comparison of the carbon^{6+} spectrum from heated and unheated Al targets. A clear reduction in proton and carbon numbers is visible. Carbon energies are enhanced due to the reduction of protons. These spectra were measured at the front of the target along the surface normal using a Thomson parabola (collection angle 2×10^{-8} sr, $B = 0.1$ T, $E =$ 3.5 kV/cm, and a CR39 detector). The numbers on the abscissa assume isotropic emission. Details on the total number of protons ($\approx 10^{12} > 1$ MeV) and their distribution can be found in [5].

center appears to contain no high energy contribution and is only visible on the low energy layer at the front of the detector stack.

The cross structure is found to be dependent on the shape, transverse size, and orientation of the target. For square targets the cross is aligned to the principal axes of the target. When the target is rotated the cross pattern rotates correspondingly. Also, the intensity of the cross pattern diminishes with increasing target size, as can be seen by comparing Figs. 2(a) and 2(d). This sets the cross pattern apart from the remaining proton signal and demonstrates that its origin is not directly related to the high energy proton signal. The protons that form the cross pattern may originate at the front of the target and then be transported around the target in a similar fashion to nanosecond duration CO_2 laser experiments [18]. An alternative explanation involving sheath acceleration from the target edges due to the field enhancement at the edges is also conceivable [19].

By contrast, the ring structure and central feature do not depend on the size and orientation of the target, and are therefore not generated in the same manner, but rather are emitted from the rear surface of the target. These two features are visible over a broad range of parameters and with fairly reproducible angular positions as indicated in Fig. 3(a). However, in this case the use of heated targets can aid our understanding of the observed signal. Figure 4 contrasts two targets consisting of 100 μm Al and 20 μm of PEEK. The top of Fig. 4 shows the data taken from a shot with the PEEK on the front of the target and the bottom shows a shot when the PEEK was on the back.

The ring structure is only clearly visible when the PEEK is on the front of the heated target. The rings in this case are quite broad, which is characteristic of plastic targets under all conditions. When the PEEK is on the rear

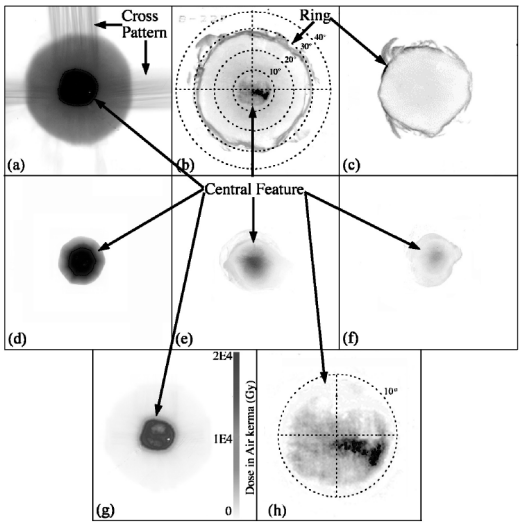

FIG. 2. (a)–(c) images from a detector stack showing the typical features observed for cold targets for $I = 10^{19}$ W cm^{-2}, 100 μm Al target. (a) Data taken using RCF film (proton energy $E \geq 3$ MeV. (b) CR39 data ($E = 5$ MeV). (c) $E = 12$ MeV (CR39). Three spatially distinct contributions are indicated. (d),(e) Series of corresponding data taken from a heated Al target under otherwise identical conditions. (d) $E \geq$ 1 MeV (RCF); (e)$E = 3$ MeV (CR39); and (f) $E = 6$ MeV (CR39). The signal level is significantly reduced on the heated target and the rings visible in (b) have (almost) disappeared. The absence of the cross pattern is due to the significantly larger spatial extent of the heated target. Angles indicated in (b) are half angles and apply to (a)–(g). (g) shows the dose derived from (a); (h) shows an enlarged view of the central feature in (b). Heavy ion contamination can be ruled out due to the proton/carbon ratio (Fig. 1) and the low carbon energies from the rear surface [20].

of the heated target the signal in the ring structure is significantly reduced and gives way to a faint signal on the CR39 as shown in Fig. 3(b). This suggests that the protons that form the rings originate on or near the front surface. Since the ring structure also contains the highest energy protons, it appears that the overall accelerating potential experienced by these protons is larger than for

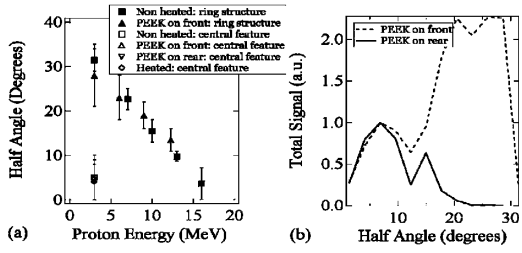

FIG. 3. (a) shows a comparison of the angular divergence of ring structure and central feature. The error bars include the variation over multiple shots and the feature width for each shot. (b) shows a comparison of the radially integrated signal for different angles for the case with PEEK on the front and PEEK on the back.

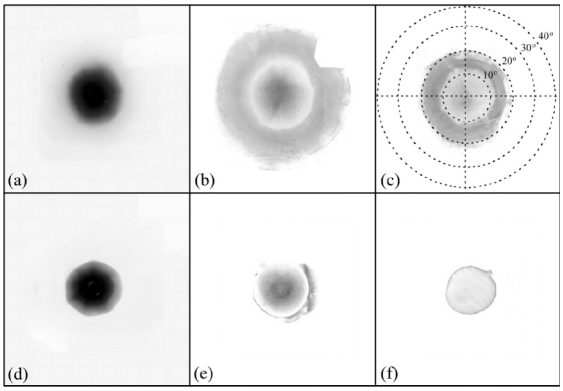

FIG. 4. Comparison of data from heated target (20 μm PEEK on 100 μm Al). The PEEK coating was on the front side in the first case (a)–(c), and on the back side of the target (d)–(f) in the second. Proton energies (a),(d) ≥ 1 MeV (RCF behind 25 μm Al filter); (b),(e) 3 MeV (CR39); (c),(f) 6 MeV (CR39). Angles indicated in (c) are half angles and apply to (a)–(f).

those at the rear of the target. The total potential may well consist of contributions from several or all the mechanisms outlined above. This result agrees well with the finding that the ring structure gives way to uniform disks of emitted protons as the target thickness is reduced below 25 μm [5]. This behavior can be understood in terms of the magnetic fields that are generated inside the solid density plasma as the electron beam propagates through it. In order to deflect all protons of a given energy by the same amount, regardless of their initial radial position, they have to pass through the same length of magnetic field. The angular spread of up to 60° full width of the rings is also in reasonably good agreement with deflection anticipated from fields predicted to be present inside the target [2]. By contrast PIC simulations predict fields at the rear of the target that are only sufficient to create structures of $<10°$ full width [13]. It is also interesting to note that the ring structure is not always centered on the target normal. Particularly for thinner targets there can be substantial deviations ($\sim 20°$) from the target normal of the ring (or disk in the case of thin targets) structure [5], providing further evidence that rings and the central feature are generated separately.

The central feature is typically responsible for the bulk of the signal at low ion energies (< 5 MeV). These low energy protons are typically well collimated ($<10°$) in contrast to the low energy component of the ring structure. This feature is reliably centered on the target normal from the rear of the target and remains visible on all shots. This suggests that the protons in the central feature originate from the rear surface of the target. It is clear from comparing Figs. 2(a)–2(c) and 2(d)–2(f) that the central feature does not extend to very high energies (although still substantial). In fact, the peak energy and the angular spread of the protons in the central feature shown in Fig. 2(h) are in very good agreement with the protons accelerated by fields at the rear of the target in detailed 3D PIC simulations [13], lending support to this interpretation of our data.

In conclusion, we have presented experimental data that allow us to distinguish between the origin of various structures present in the energetic proton signal at the rear of the target in high power laser-solid interactions. We have identified three distinct proton populations that contribute to the signal observed on the detectors. First, the cross structure that is separate from the high energy component. Second, the ring structure that contains the highest energy particles for our conditions consists of protons that originate from or near the front surface, strongly supporting the original hypothesis by Clark *et al.* [2]. Third, the low divergence, lower energy central feature originates at the rear of the target and agrees well in structure and energy with simulation results for protons accelerated from the rear surface [13]. It is also in reasonable agreement with the data published for rear surface acceleration in the recent publication by Hegelich *et al.* [20].

The authors acknowledge the assistance of the Rutherford Appleton Laboratory staff, AWE target fabrication group, and the support of the EPSRC.

*Email address: m.zepf@qub.ac.uk

[1] A. Modena *et al.*, Nature (London) **377**, 606 (1995); E. Esarey *et al.*, IEEE Trans. Plasma Sci. **24**, 252 (1996).
[2] E. L. Clark *et al.*, Phys. Rev. Lett. **84**, 670 (2000).
[3] R. Snaveley *et al.*, Phys. Rev. Lett. **85**, 2945 (2000).
[4] A. Maksimchuk *et al.*, Phys. Rev. Lett. **84**, 4108 (2000); K. Nemoto *et al.*, Appl. Phys. Lett. **78**, 595 (2001).
[5] M. Zepf *et al.*, Phys. Plasmas **8**, 2323 (2001).
[6] S. C. Wilks *et al.*, Phys. Rev. Lett. **69**, 1383 (1992); E. L. Clark *et al.*, Phys. Rev. Lett. **85**, 1654 (2000).
[7] C. Toupin *et al.*, Phys. Plasmas **8**, 1011 (2001).
[8] L. Disdier *et al.*, Phys. Rev. Lett. **82**, 1454 (1999); P. A. Norreys *et al.*, Plasma Phys. Controlled Fusion **40**, 175 (1998).
[9] J. T. Mendonca *et al.*, Meas. Sci. Technol. **12**, 1801 (2001); J. R. Davies, Laser Part. Beams **20**, 243 (2002).
[10] A. R. Bell *et al.*, Plasma Phys. Controlled Fusion **39**, 653 (1997).
[11] J. R. Davies *et al.*, Phys. Rev. E **56**, 7193 (1997).
[12] Y. Sentoku *et al.*, Appl. Phys. B **74**, 207 (2002).
[13] A. Pukhov, Phys. Rev. Lett. **86**, 3562 (2001).
[14] M. Tatarakis *et al.*, Phys. Rev. Lett. **81**, 999 (1998); M. Borghesi *et al.*, Phys. Rev. Lett. **83**, 4309 (1999).
[15] M. G. Haines, Phys. Rev. Lett. **78**, 254 (1997).
[16] A. J. MacKinnon *et al.*, Phys. Rev. Lett. **86**, 1769 (2001).
[17] S. J. Gitomer *et al.*, Phys. Fluids **29**, 2679 (1984).
[18] R. Marjoribanks *et al.*, Phys. Rev. Lett. **45**, 1798 (1980).
[19] A. J. MacKinnon (private communication).
[20] M. Hegelich *et al.*, Phys. Rev. Lett. **89**, 085002 (2002).